A GPU approach to real-time coherence-based photoacoustic imaging and its application to photoacoustic visual servoing

Gonzalez, Eduardo, Bell, Muyinatu

Eduardo Gonzalez, Muyinatu A. Lediju Bell, "A GPU approach to real-time coherence-based photoacoustic imaging and its application to photoacoustic visual servoing," Proc. SPIE 11240, Photons Plus Ultrasound: Imaging and Sensing 2020, 1124054 (17 February 2020); doi: 10.1117/12.2546023

SPIE.

Event: SPIE BiOS, 2020, San Francisco, California, United States

A GPU approach to real-time coherence-based photoacoustic imaging and its application to photoacoustic visual servoing

Eduardo Gonzalez[a] and Muyinatu A. Lediju Bell[a,b,c]

[a]Department of Biomedical Engineering, Johns Hopkins University, Baltimore, MD, USA
[b]Department of Electrical and Computer Engineering, Johns Hopkins University, Baltimore, MD, USA
[c]Department of Computer Science, Johns Hopkins University, Baltimore, MD, USA

ABSTRACT

Vision-based robotic control (also known as visual servoing) is promising for surgical tool tip tracking and automated visualization of photoacoustic targets during interventional procedures. However, reliable segmentation in photoacoustic-based visual servoing was previously achieved with a light source that exceeds laser safety limits, due to the limited availability of laser safety limits for only skin or eyes and the associated difficulty with visualizing signals at the low laser energies within these safety limits for millimeter-sized light sources. Short-lag spatial coherence (SLSC) imaging is an advanced beamforming method that has shown offline promise toward enhancing the visualization of signals acquired with low laser energies. This paper summarizes the first known GPU-based, real-time implementation of SLSC for photoacoustic imaging and displays example images showing the application of this real-time algorithm to improve signal visualization and segmentation for visual servoing tasks. Results with *ex vivo* bovine tissue demonstrate that real-time SLSC imaging recovers signals obtained with low laser energies (i.e., ≤ 268 μJ) with mean $\pm$ standard deviation signal-to-noise ratios (SNRs) of 11.2 ± 2.4 (compared to 3.5 ± 0.8 with conventional delay-and-sum beamforming). Therefore, real-time SLSC imaging enables low laser energies for visual servoing within existing safety limits, which is promising for multiple surgical interventions.

1. INTRODUCTION

Vision-based robot control (also known as visual servoing) is a promising technique to maintain visualization of surgical tool tips, with the "vision" provided by photoacoustic data. In this technique, an ultrasound probe attached to a robot arm receives photoacoustic signals from a tool tip. An image segmentation algorithm then locates the source of the photoacoustic signals. Finally, the ultrasound probe motion is controlled by the robot to ensure that the tool tip remains at the center of the image,[1] and this process is repeated as the tool tip moves during a procedure.

Previous studies focused on photoacoustic-based visual servoing with conventional delay-and-sum (DAS) beamforming.[1] However, DAS images have poor signal-to-noise ratio (SNR) in the presence of low laser energies and exhibit side lobe artifacts at high laser energies, which both compromise the performance of the segmentation algorithm during visual servoing. These limitations may be overcome by increasing the laser energy or otherwise enhancing the amplitude of photoacoustic signals. For example, frame averaging may be applied to enable the use of lower energies and simultaneously reduce incoherent noise and artifact. However, this option introduces motion blurring and reduces frame rates, which both have negative impacts on the tracking accuracy and efficacy of real-time visual servoing.[2]

Short-lag spatial coherence (SLSC) imaging is an advanced beamforming technique that was originally developed for ultrasound imaging to directly display measurements of the spatial coherence rather than amplitude.[3] When applied to photoacoustic imaging, SLSC beamforming has been shown to enhance the contrast of targets without frame averaging, as well as enhance the quality of photoacoustic signals acquired with low laser energies.[4] This enhancement is advantageous because the use of low laser energies is often necessary to ensure laser safety and miniaturized low-energy light delivery systems, such as pulsed laser diodes,[4] which are beneficial for portability in the operating room.

Photons Plus Ultrasound: Imaging and Sensing 2020, edited by Alexander A. Oraevsky, Lihong V. Wang,
Proc. of SPIE Vol. 11240, 1124054 · © 2020 SPIE · CCC code: 1605-7422/20/$21 · doi: 10.1117/12.2546023

This paper summarizes the first known real-time implementation of SLSC beamforming for photoacoustic imaging applied on a FDA-approved clinical and research ultrasound Alpinion E-CUBE 12R system[5] and provides example images showing the application of this real-time implementation to improve visual servoing. Although performance is demonstrated with a solid state laser as the initial light source, success was achieved with energies low enough to replace this light source with a pulsed laser diode.

2. METHODS & MATERIALS

2.1 GPU Implementation

The overall process for real-time photoacoustic-based visual servoing is illustrated in Fig. 1. The main steps include acquisition of a photoacoustic image in real time, segmentation of the photoacoustic target (e.g., a needle, tool, or catheter tip) through a series of morphological operations and filtering, calculation of the global position of the centroid of the segmented target, and finally commanding the robot to center the ultrasound probe on the segmented target.

In contrast to the real-time DAS photoacoustic images that have been implemented to demonstrate photoacoustic-based visual servoing to date,[1,6] real-time SLSC photoacoustic images were achieved by using the graphical processing unit (GPU) device embedded in the same Alpinion E-CUBE 12R ultrasound system (Alpinion, Medical Systems, Seoul, Korea) used to acquire the DAS photoacousic data. To implement real-time SLSC imaging on this device, raw channel data were acquired by the ultrasound system, which was triggered by a signal from a Phocus Mobile laser system (Opotek Inc., Carlsbad, CA, USA). This laser system was comprised of a solid state Nd:YAG laser coupled to an optical parametric oscillator to enable variable wavelengths outside of the 1064 nm primary wavelength of the Nd:YAG laser.

After ordering the resulting raw data and storing the ordered photoacoustic data in texture memory, DC removal was computed with 1D convolutions of time-domain kernels executed independently along the axial dimension. The Hilbert transform was then computed along the axial dimension using the fast Fourier transform (FFT) libraries embedded in the compute unified device architecture (CUDA) (NVIDIA, Santa Clara, CA, USA). Next, synthetic receive aperture imaging was implemented to generate a specific number of scanlines determined by the user as an input parameter.

The SLSC beamforming computations "Coherence factors" and "Spatial compounding" shown in Fig. 1 were previously implemented by Hyun *et al.*[7] for ultrasound imaging with a Verasonics ultrasound system.[8] In contrast to the original SLSC beamformer,[3] the estimator computes a single ensemble correlation coefficient

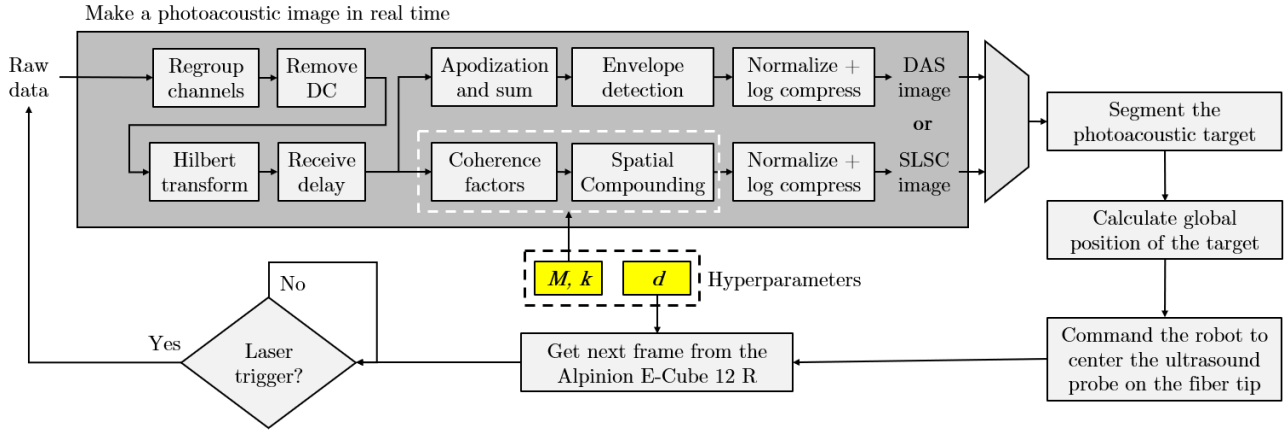

Figure 1: Flow diagram of the photoacoustic-based visual servoing algorithm with real-time delay-and-sum (DAS) and real-time short-lag spatial coherence (SLSC) beamforming. The display of either an SLSC image or a DAS image is pre-determined by the user. The cumulative lag M and averaging kernel k determine the quality of the SLSC images, while the image depth d determines the amount of data to process for both DAS and SLSC beamforming.

from ensemble coherence factors rather than an average over all element pairs separated by a lag m. Then, the coherence factors are compounded across a spatial kernel k and a cumulative lag M. The values M=25, k=11, and an overall image depth, d, of 5 cm were chosen for the results presented in this paper.

Finally, negative SLSC values were set to zero,[9] and the resulting SLSC image was normalized and log-compressed. The maximum term for normalization was computed using logarithmic reduction strategies.[10] This GPU-SLSC implementation was executed on a GeForce GTX 1080 GPU (NVIDIA Corporation, Santa Clara, CA, USA) with 8GB of VRAM and a core clock speed of 1733 MHz.

2.2 Image Quality Assessments

A 1 mm-core-diameter optical fiber was coupled to the Phocus Mobile laser source on one end with the other end inserted into *ex vivo* bovine muscle at an axial depth, s, of 2.5 cm. The laser coupled to the optical fiber transmitted 900 nm wavelength light. A L3-8 linear array ultrasound probe was attached to a Sawyer robot (Rethink Robotics, Boston, MA) on one end and connected to the ultrasound system on the other end. This probe was acoustically coupled to the top of the *ex vivo* tissue, so that the length of the optical fiber was aligned with the elevation axis of the probe.

The experimental setup described above was used to determine the minimum possible energy limits for SLSC beamforming in comparison to DAS beamforming. Given the 1 mm-core-diameter optical fiber geometry and the current standards for skin,[11] the maximum permissible exposure (MPE) was 50 μJ/cm^2. This MPE translates to a maximum energy safety limit of 400 μJ. The laser energy was varied above and below the MPE (i.e., laser energies of 118, 184, 268, 364, 463, 570, and 645 μJ) for multiple photoacoustic image acquisitions.

For each these laser energies, GPU-SLSC images and the corresponding raw data were stored on the host computer. In order to compare the fidelity of GPU-SLSC to the original algorithm, the stored raw data was processed off-line on the host CPU of the Alpinion E-CUBE 12R system to create CPU-SLSC images. The host CPU had a Intel Xeon E5-1620 processor with 3.5 GHz clock speed and 32 GB of RAM. Similarly, DAS images were also created off-line on the host CPU from the acquired raw data for additional comparison.

The resulting GPU-SLSC, CPU-SLSC, and DAS image SNR for each laser energy was evaluated as follows:

$$\mathrm{SNR} = \frac{\mu_i}{\sigma_o}, \tag{1}$$

where μ_i is the mean value within a ROI inside of the photoacoustic target and σ_o is the standard deviation within a ROI outside of the target.

2.3 Visual servoing of a fiber tip inserted in *ex vivo* bovine muscle

Using the same experimental setup described in Section 2.2, the probe centering experiment described by Bell and Shubert[1] was used to assess the performance of real-time GPU-SLSC imaging in comparison to real-time DAS imaging for the visual servoing task. The length of the optical fiber was aligned with the imaging plane for this assessment. The tip of the optical fiber, located at 2.5 cm axial depth, was laterally displaced 6 mm from the center of the image. The visual servoing algorithm described in Section 2.1 was then activated, and the robot was commanded to maintain the lateral center of the probe on the fiber tip. This probe centering experiment was performed with laser energies above (i.e., 645 μJ) and below (i.e., 110 μJ) the energy safety limit of 400 μJ.

3. RESULTS

3.1 SNR vs. laser energies in *ex vivo* tissue

Fig. 2(a) shows examples of photoacoustic images of the fiber tip acquired with 268 μJ laser energy. The mean $\pm$ one standard deviation SNR for off-line DAS, CPU-SLSC, and GPU-SLSC imaging was 3.5 $\pm$ 0.9 dB, 11.4 $\pm$ 2.9 dB, 12.1 $\pm$ 4.2 dB, respectively. Fig. 2(b) shows the quantitative results of the SNR measurements as a function of energy. Combining both CPU and GPU versions, SLSC imaging consistently outperformed DAS imaging and visualized photoacoustic signals acquired with low laser energies ($\leq$ 268 μJ) with a mean SNR of 11.2 $\pm$ 2.4 when compared to that of DAS imaging (i.e., 3.5 $\pm$ 0.8). In addition, the mean $\pm$ one standard deviation of the SNR difference between the CPU-based and GPU-based SLSC implementations was 1.14 $\pm$ 3.99.

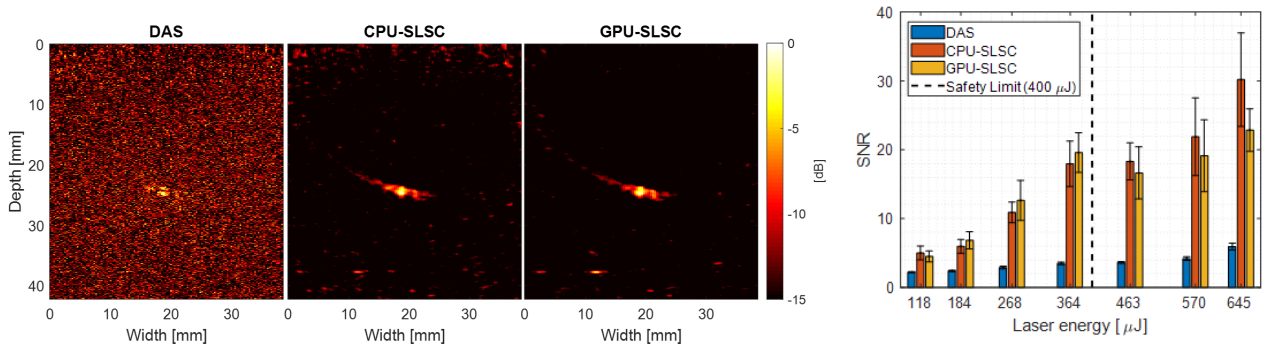

(a) (b)

Figure 2: Photoacoustic signals from an optical fiber inserted into *ex vivo* bovine muscle. (a) Example of photoacoustic images with 268 μJ laser energy. Images were normalized, log-compressed, and displayed with a dynamic range of 15 dB. (b) SNR results of the photoacoustic target as a function of laser energy.

3.2 Probe centering in *ex vivo* bovine muscle

Fig. 3 shows photoacoustic images for probe centering tests operating at low and high laser energies (i.e., 110 μJ and 645 μJ, respectively). The segmented target denoted by the blue circle is present and constant for both DAS and SLSC images at 645 μJ. The "Before" column for this energy shows the initial position of the fiber before the visual servoing algorithm was executed. The "After" column shows the final position after the probe centering task was completed. Overall, visual servoing using both DAS and GPU-SLSC beamformers successfully accomplished the probe centering task with the high laser energy. In contrast, for the low laser energy, the example in Fig. 3 shows that visual servoing with DAS failed to segment the target due to the low SNR, while visual servoing with SLSC imaging enhances the SNR and the target was successfully segmented to complete the probe centering task.

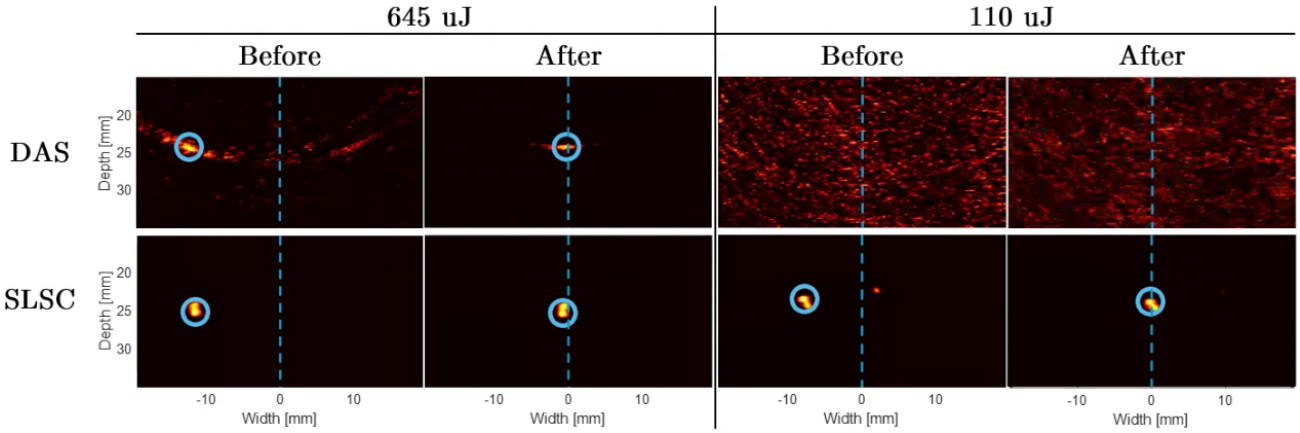

Figure 3: Example probe centering results for high and low laser energies before and after the visual servoing task is completed. The dashed blue line denotes the center of the image and the blue circle denotes the detected target by the segmentation algorithm within the visual servoing system.

4. DISCUSSION

Photoacoustic signals acquired with low laser energies were improved with GPU-SLSC imaging. The current optical fiber and laser configuration had a laser safety limit of 400 μJ, which is determined by the diameter of the optical fiber and wavelength of excitation. As GPU-SLSC imaging performed well with laser energies as low as 118μJ, these results indicate that visual servoing with GPU-SLSC imaging will benefit from the introduction

of smaller and more portable light delivery systems, which are advantageous for performing visual servoing in the operating room.

Typically, visual servoing methods include a search algorithm that is triggered when a series of unsuccessful segmentation events is recorded.[6] As suggested by Fig. 3, an unsuccessful search algorithm is expected to be initiated for the low-energy example with DAS imaging. In the worst case scenario, a non-converging search motion of the ultrasound probe hinders the effective operating area of surgeons, which adds delays to the overall procedure. GPU-SLSC imaging has the potential to mitigate these scenarios.

5. CONCLUSION

Real-time SLSC beamforming for photoacoustic imaging was implemented on a GPU utilizing parallel processing techniques. *Ex vivo* results with bovine tissue demonstrate that GPU-SLSC imaging recovered signals at low laser energies, which is promising for the miniaturization of lasers to perform photoacoustic-based visual servoing in the operating room or interventional suite. In addition, the presented visual servoing results indicate that GPU-SLSC imaging is superior to DAS imaging when performing probe centering with low laser energies.

ACKNOWLEDGMENTS

The authors acknowledge the support of NVIDIA Corporation with the donation of the Titan Xp GPU used for this research and Dongwoon Hyun for sharing SLSC GPU example code specific to the Verasonics ultrasound imaging system.

REFERENCES

[1] Bell, M. A. L. and Shubert, J., "Photoacoustic-based visual servoing of a needle tip," *Scientific Reports* **8**(1), 15519 (2018).

[2] Jespersen, S. K., Wilhjelm, J. E., and Sillesen, H., "In vitro spatial compound scanning for improved visualization of atherosclerosis," *Ultrasound in Medicine & Biology* **26**(8), 1357–1362 (2000).

[3] Lediju, M. A., Trahey, G. E., Byram, B. C., and Dahl, J. J., "Short-lag spatial coherence of backscattered echoes: Imaging characteristics," *IEEE Transactions on Ultrasonics, Ferroelectrics, and Frequency Control* **58**(7) (2011).

[4] Bell, M. A. L., Guo, X., Kang, H. J., and Boctor, E., "Improved contrast in laser-diode-based photoacoustic images with short-lag spatial coherence beamforming," in [*2014 IEEE International Ultrasonics Symposium*], 37–40, IEEE (2014).

[5] Gonzalez, E., Gubbi, M. R., and Bell, M. A. L., "GPU implementation of coherence-based photoacoustic beamforming for autonomous visual servoing," in [*2019 IEEE International Ultrasonics Symposium (IUS)*], 24–27, IEEE (2019).

[6] Graham, M., Assis, F., Allman, D., Wiacek, A., Gonzalez, E., Gubbi, M., Dong, J., Hou, H., Beck, S., Chrispin, J., and Bell, M. A. L., "In vivo demonstration of photoacoustic image guidance and robotic visual servoing for cardiac catheter-based interventions," *IEEE Transactions on Medical Imaging* (2019).

[7] Hyun, D., Crowley, A. L. C., and Dahl, J. J., "Efficient strategies for estimating the spatial coherence of backscatter," *IEEE Transactions on Ultrasonics, Ferroelectrics, and Frequency Control* **64**(3), 500–513 (2016).

[8] Hyun, D., Crowley, A. L. C., LeFevre, M., Cleve, J., Rosenberg, J., and Dahl, J. J., "Improved visualization in difficult-to-image stress echocardiography patients using real-time harmonic spatial coherence imaging," *IEEE Transactions on Ultrasonics, Ferroelectrics, and Frequency Control* **66**(3), 433–441 (2018).

[9] Bell, M. A. L., Goswami, R., Kisslo, J. A., Dahl, J. J., and Trahey, G. E., "Short-lag spatial coherence imaging of cardiac ultrasound data: Initial clinical results," *Ultrasound in Medicine & Biology* **39**(10), 1861–1874 (2013).

[10] Cook, S., [*CUDA programming: a developer's guide to parallel computing with GPUs*], Newnes (2012).

[11] American National Standards Institute, "American national standard for the safe use of lasers," (2007).